EES Batteries

ROYAL SOCIETY OF CHEMISTRY

PAPER

View Article Online
View Journal | View Issue

Open Access Article. Published on 15 July 2025. Downloaded on 12/12/2025 10:12:56 PM.
This article is licensed under a Creative Commons Attribution-NonCommercial 3.0 Unported Licence.

Check for updates

Cite this: *EES Batteries*, 2025, **1**, 1173

Stable, high-rate, organic zinc-ion batteries accomplished using an ion-conducting marine-inspired binder†

Alicia M. Battaglia,[a] Jiang Tian Liu,[a] Victor Lotocki,[a] Kristen L. Perry[a] and Dwight S. Seferos *[a,b]

Received 4th July 2025,
Accepted 11th July 2025

DOI: 10.1039/d5eb00125k

rsc.li/EESBatteries

Aqueous zinc-ion batteries (AZIBs) are promising for a range of future energy storage needs. However, their widespread adoption is hindered by the cathode's poor conductivity and high solubility in the aqueous electrolyte, resulting in low energy density and poor cycle life. Most research has focused on improving the active material performance, with less emphasis on optimizing other electrode components. Binders, which are essential for maintaining electrode integrity during cycling, can also play a crucial role in enhancing conductivity and mitigating dissolution. In this study, we introduce a novel dual-functional polymer, POxa**PG**, incorporating gallol (a marine adhesive) and polyethylene gallol (PEG) as a binder that addresses these challenges. Due to the strong adhesion and excellent mechanical stability provided by the robust bonding between the gallol groups and the carbonyl active material, and high ionic conductivity provided by the PEG groups, an organic AZIB incorporating this binder achieves capacities ranging from ~350 mAh g^{-1} (0.01 A g^{-1}) to 200 mAh g^{-1} (20 A g^{-1}), among the highest reported for organic materials at these rates. Furthermore, the cathode with the conductive gallol binder demonstrates exceptional cycling performance compared to electrodes using the conventional polyvinylidene fluoride (PVDF) binder, demonstrating outstanding capacity retention after over 8000 cycles at 1 A g^{-1}. This work provides a valuable new approach for designing adhesive, conductive, and environmentally-friendly binders, thereby enhancing the commercial potential of organic materials in AZIBs.

Broader context

The development of secondary battery technologies, such as organic zinc-ion batteries, is crucial for transitioning to sustainable energy storage and minimizing the environmental impact of Li-ion batteries. The cathode material is the key component of the battery and plays a critical role in determining overall battery performance. Given the various challenges encountered by cathode materials under practical operation, specifically poor conductivity and high solubility in liquid electrolytes, the importance of the binder cannot be overlooked. Commercial binders like polyvinylidene fluoride (PVDF) and polytetrafluoroethylene (PTFE) are commonly used, but they suffer from significant drawbacks including weak adhesion, low conductivity, and their classification as per- and polyfluoroalkyl substances (PFAS). In this study, a novel ion-conductive marine-inspired binder that is fluorine-free and possesses strong adhesion is designed to address these main issues that plague organic cathodes in aqueous zinc-ion batteries. The new binder maintains firm adhesion of the cathode components in the aqueous electrolyte, resulting in stable cycling for over 8000 cycles at 1 A g^{-1}. Additionally, the incorporation of ion-conductive groups compensates for the typical poor ion-conductivity of organic materials, thereby improving the Zn^{2+} diffusion and leading to one of the highest capacities for batteries of this type reported to date. Our findings are applicable to other types of materials for aqueous zinc-ion batteries, such as sulfides, covalent organic frameworks, organic radicals, and conjugated polymers, and can likely be extended to other ion battery types.

Introduction

Clean energy offers a solution to the energy crisis and global warming driven by CO_2 emissions, making it a topic of widespread interest. However, the deployment of clean energy sources like wind and solar is often hindered by their uneven geographic distribution and intermittent supply. To address this, large-scale energy storage systems are essential for effectively harnessing and utilizing green energy. Lithium-ion bat-

[a]*Department of Chemistry, University of Toronto, 80 St. George Street, Toronto, Ontario, M5S 3H6, Canada. E-mail: dwight.seferos@utoronto.ca*
[b]*Department of Chemical Engineering and Applied Chemistry, University of Toronto, 200 College Street, Toronto, Ontario, M5S 3E5, Canada*
† Electronic supplementary information (ESI) available. See DOI: https://doi.org/10.1039/d5eb00125k

© 2025 The Author(s). Published by the Royal Society of Chemistry

Open Access Article. Published on 15 July 2025. Downloaded on 12/12/2025 10:12:56 PM.
This article is licensed under a Creative Commons Attribution-NonCommercial 3.0 Unported Licence.

teries (LIBs) are the most widely used energy storage technology, dominating portable electronics and electric vehicle markets. However, concerns about the scarcity and high cost of lithium and other critical metals, the toxicity of the electrolytes, and safety risks pose significant challenges, particularly for large-scale applications.[1–3] These issues have dramatically increased the search for alternative, cost-effective energy storage solutions that are based on abundant metals. Among these alternatives, rechargeable aqueous zinc-ion batteries (AZIBs) have gained considerable attention for large-scale energy storage due to the high theoretical capacity of zinc (5855 mAh cm^{-3}), low cost (less than $100 per kWh compared to other aqueous batteries), and enhanced safety by using near-neutral or weak acidic electrolytes.[4,5] Despite their potential, several challenges remain unresolved, such as the low plating-stripping coulombic efficiency, dendrite growth of the Zn metal anode, and poor cycle stability of the cathode materials.[6–9]

Of the various cathode materials that can be used in AZIBs, carbonyl compounds (*i.e.* quinones, imides, and carboxylates) have garnered significant interest as redox-active materials due to their numerous advantages, including high theoretical capacity, excellent electrochemical reversibility, structural diversity, and molecular tunability.[10–12] Despite their promising attributes, carbonyl materials face several challenges that limit their practical capacities. First, they often suffer from poor electrical conductivity, thus requiring a significant amount of conductive additives during electrode fabrication, which in turn reduces their energy density. Additionally, the high solubility of carbonyl materials in aprotic organic electrolytes leads to capacity fading and poor cycle life.[10,13] Several strategies have been investigated to address these issues, such as incorporating functional groups (–NH_2, –CH_3, –F, *etc.*) into the carbonyl structure,[14–18] forming polymers[19,20] or salts,[21] or applying them to solid-state battery systems.[22–24] As useful as these strategies are, most are focused on modifying the redox-active materials, with little attention being afforded to the binder. It should be noted that the binder is responsible for holding the electrode materials together, facilitating efficient electron and ion transport, and ensuring good adhesion to the current collector. Thus, the importance of the binder should not be overlooked.

The development of AZIBs is still in its infancy.[25] Presently, most AZIB electrodes use polyvinylidene fluoride (PVDF) as the binder since it is commercially available and provides reasonable chemical and electrochemical stability.[26] However, PVDF is insulating, consequently occupying precious volume in the electrode without providing any additional conductivity to the composite. PVDF is also derived from fluorinated compounds, which are environmentally harmful and challenging to dispose of or recycle.[27] Lastly, PVDF binds through weak van der Waals forces.[26,28] Although van der Waals forces are generally adequate for most conventional intercalation-based electrodes, they do not provide optimal adhesion for organic active materials and could potentially lead to reduced mechanical integrity and electrode performance. Researchers have explored various water-based binders, such as sodium alginate (SA), carboxymethyl cellulose (CMC), and cellulose acetate, as potential alternatives for PVDF in AZIBs because of their exceptional adhesive properties.[29,30] However, these water-based binders may face challenges with solubility stability in aqueous electrolytes. Given that organic carbonyl electrodes suffer from poor conductivity and high solubility in the electrolyte, it is crucial to develop a binder that is both conductive and has improved binding affinity for the carbonyl active material in water-based electrolytes.

Inspired by the ability of marine life (including mussels' and other mollusks) to adhere to diverse surfaces in complex, high ionic strength environments, catechol-containing polymers have garnered significant attention as binders, particularly for silicon anodes.[31–35] Compared to catechols, gallols have an additional hydroxyl group on the aromatic ring, and have demonstrated even stronger adhesion across various conditions, especially in aqueous environments.[36] These superior adhesive properties arise from the multiple molecular interactions that gallols can participate in, including hydrogen bonding, coordination bonding, and π–π interactions with different components. They are also abundant in natural sources such as gallnuts, tea leaves, as well as the aforementioned marine organisms (tunicates), providing a more sustainable alternative to the standard toxic, halogenated commercial binder, PVDF. Despite these advantages, gallol-based compounds have only been investigated as binders for silicon anodes,[37–39] leaving their potential as cathode binders unexplored. Given their strong adhesion, particularly in aqueous conditions, we postulated that they could also serve as effective binders for organic cathodes in AZIBs.

In this work, we show that AZIBs can be enhanced using a novel conductive polymeric binder, POxa**PG**, that contains gallol and polyethylene glycol (PEG) pendant groups. This polymer was designed, prepared, and tested as a binder for carbonyl-based cathodes (Fig. 1). The gallol functional group can provide strong adhesion to the carbonyl active material, thus preventing its dissolution during battery cycling. Meanwhile, the ionic conductive nature of the oxanorbornene backbone and PEG pendant group were expected to enhance the material's conductivity, thus increasing the capacities of the battery. For comparison, we also prepared polymer binders containing only gallol or PEG pendant groups to investigate the contribution of each moiety to the overall performance of the cell, as well as a PVDF control. Overall, the results demonstrate that careful binder design will significantly enhance the performance of AZIBs.

Results and discussion

Design and characterization of the POxaPG binder

The conductive gallol polymer, POxa**PG**, was prepared in four steps from commercial sources (Fig. 2a, see ESI† for details). First, the phenol groups of gallic acid were protected with acetyl groups (Fig. S1 and S2†).[40] This was necessary to both

 © 2025 The Author(s). Published by the Royal Society of Chemistry

Open Access Article. Published on 15 July 2025. Downloaded on 12/12/2025 10:12:56 PM.
This article is licensed under a Creative Commons Attribution-NonCommercial 3.0 Unported Licence.

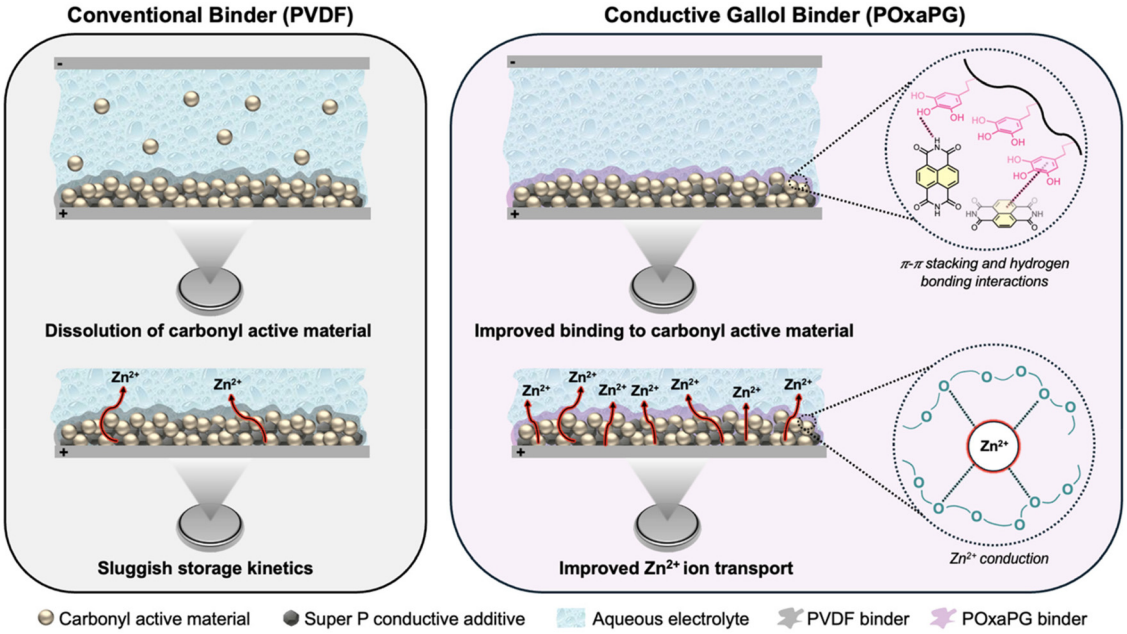

Fig. 1 Schematic depiction of the operation of the binders in the study in coin-type AZIBs: (Left) the conventional binder, PVDF; (Right) the novel conductive gallol binder, POxa**PG**. The illustration highlights the key challenges associated with PVDF and how POxa**PG** is designed to mitigate these issues.

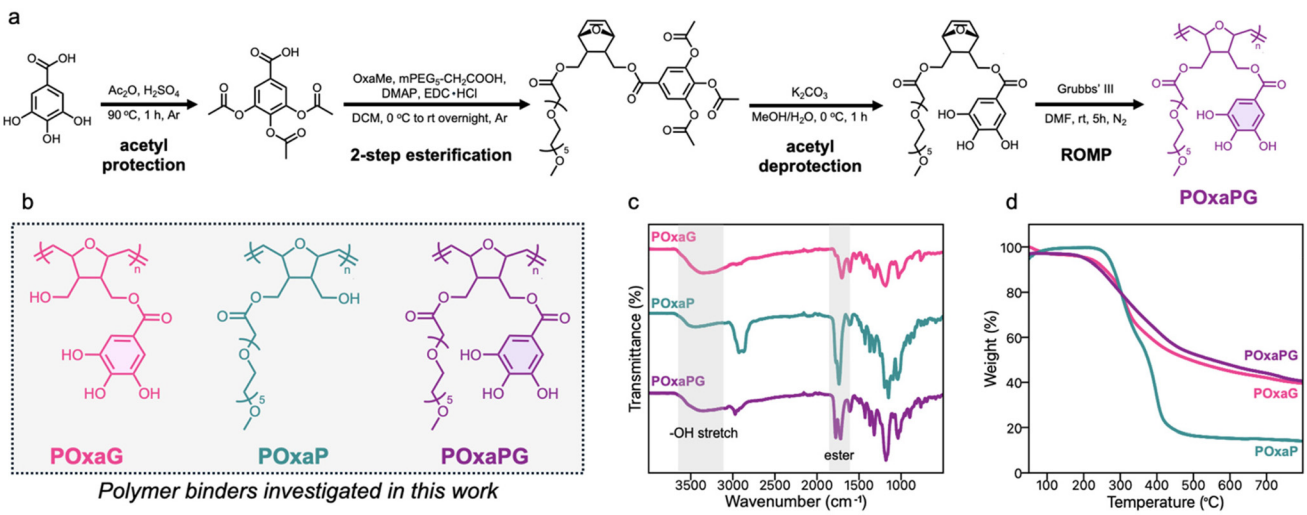

Fig. 2 (a) General scheme for the synthesis of POxaPG through acetyl protection, esterification, acetyl deprotection, and ring-opening metathesis polymerization. (b) Chemical structures of the polymer binders investigated in this work. (c) FTIR spectra of the polymers. (d) Thermal gravimetric analysis (TGA) of the polymers at a heating rate of 10 °C min^{-1} under N_2.

protect the hydroxyl groups from oxidizing during subsequent steps, and to ensure that only the carboxylic acid group reacted with the oxanorbornene during Steglich esterification. In addition, the increased electron-donating ability of the unprotected phenols, relative to the acetylated form, hinder esterification. Next, Steglich esterification was performed twice on the oxanorbornene monomer: first, to attach the protected gallol moiety onto the oxanorbornene backbone, and second, to link the PEG chain to the monomer backbone (Fig. S9 and S10†). The acetyl protecting groups were removed from the gallol moiety using mild basic conditions (Fig. S12†).

Characterization of this monomer using Fourier Transform Infrared spectroscopy (FTIR) provides evidence for the successful deprotection of the acetyl groups from the gallol moiety (Fig. S16†). Upon deacetylation, the –OH stretch from 3050–3700 cm^{-1} becomes more pronounced, resulting from the presence of the pendant gallol moiety and the removal of the acetyl groups. Additionally, the absence of the acetyl peak

Open Access Article. Published on 15 July 2025. Downloaded on 12/12/2025 10:12:56 PM.
This article is licensed under a Creative Commons Attribution-NonCommercial 3.0 Unported Licence.

at 2.3 ppm in the ^{1}H NMR spectra provides further confirmation of complete acetyl deprotection (Fig. S12†).

The oxanorbornene unit of the monomer was then polymerized by ring-opening metathesis polymerization using Grubbs' third generation catalyst.[41] The polymerization was conducted at room temperature using a [monomer] : [catalyst] ratio of 25 : 1 and a monomer concentration of 0.02 M. ^{1}H NMR spectra (Fig. S15†) provide evidence that the polymerization was complete. The alkene peaks at 6.4 ppm disappeared and new broad signals, corresponding to the polymer backbone, appear at 5.6 ppm. A general broadening of peaks was also observed, indicating polymer formation.

Homopolymers containing either gallol or PEG moieties, POxa**G** and POxa**P**, were also synthesized to evaluate the individual contribution of each functional group to AZIB performance (Fig. 2b). Similar synthetic methodologies were employed (see ESI† for details). All polymers were synthesized with the same monomer : initiator ratio for accurate comparison.

Characterization using FTIR provides further evidence for the successful synthesis of the three polymers (Fig. 2c). A broad O–H stretch from 3050–3700 cm^{-1} is observed for all polymers, arising from the pendant gallol and/or PEG groups. The C–H stretching bands of the alkanes in the PEG groups can be seen at 2900 cm^{-1} in POxa**P** and POxa**PG**. Finally, the ester C═O band at ~1700 cm^{-1} can be observed for all polymers. Optical absorption spectroscopy was used to verify that the gallol groups did not oxidize upon polymerization. Both polymers, POxa**G** and POxa**PG**, show a distinct band around 274 nm, attributed to the pendant gallol groups (Fig. S18†). Moreover, the lack of a broad absorption band between 350–500 nm indicates that oxidation did not occur.[42] Finally, the thermal properties of the polymers was assessed using thermal gravimetric analysis (TGA) (Fig. 2d). POxa**G** and POxa**PG** show similar onsets of degradation around 210 °C. In contrast, POxa**P** shows a slightly higher degradation temperature of 260 °C, but exhibits a more pronounced loss. Nevertheless, all polymers demonstrate adequate thermal stability for their use as AZIB binder materials.

Cathode preparation and properties

Composite cathodes were prepared using 1,4,5,8-naphthalene diimide (NTCDI) as the active material, Super P as the conductive additive, and a polymer binder (either PVDF, POxa**G**, POxa**P**, or POxa**PG**) at a weight ratio of 60 : 30 : 10 (Fig. 3a). NTCDI was selected as the redox-active material due to its excellent electron-accepting abilities and insolubility in aqueous electrolytes. NTCDI can also participate in hydrogen bonding and π–π stacking with the gallol moiety, thus providing stronger adhesion compared to PVDF.[39,43,44] To facilitate sufficient interaction between the active material and binder,

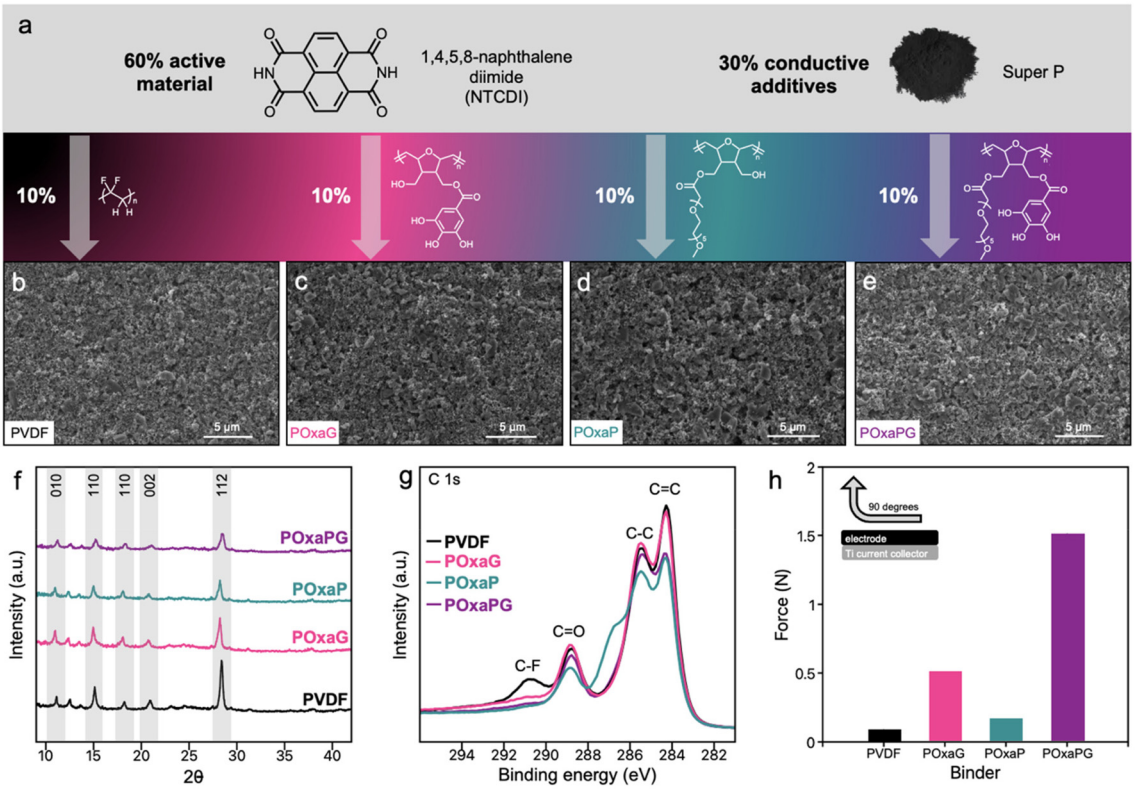

Fig. 3 (a) Chemical structure and schematic of the cathode compositions. Corresponding SEM images of cathodes using (b) PVDF, (c) POxa**G**, (d) POxa**P**, or (e) POxa**PG** binders. (f) pXRD patterns of pristine cathodes with PVDF, POxa**G**, POxa**P**, or POxa**PG** binders. (g) C 1s XPS spectra of pristine cathodes with PVDF, POxa**G**, POxa**P**, or POxa**PG** binders. (h) Average peeling force over 40 mm displacement of cathodes with PVDF, POxa**G**, POxa**P**, or POxa**PG** binder.

 © 2025 The Author(s). Published by the Royal Society of Chemistry

Open Access Article. Published on 15 July 2025. Downloaded on 12/12/2025 10:12:56 PM.
This article is licensed under a Creative Commons Attribution-NonCommercial 3.0 Unported Licence.

cathodes containing the oxanorbornene polymers were first dissolved in methanol (for POxa**G** or POxa**PG**) or chloroform (for POxa**P**) and stirred overnight with Super P. As PVDF is already highly soluble in the cathode slurry solvent, NMP, PVDF was not subjected to the premixing treatment. The cathode slurries were blade-coated onto stainless steel current collectors using a notch bar with a height of 200 μm.

The morphology of the cathodes was compared using scanning electron microscopy (SEM) (Fig. 3b–e). All cathodes have a uniform distribution of the active material and binder within the carbon matrix, suggesting that the choice of binder does not affect the dispersion characteristics of the cathodes. Optimal cathode architectures should feature an even distribution of active particles throughout the conductive network of the cathode to ensure uniform utilization of the active material. Additionally, uniformly distributed low-resistance internal pathways are essential to facilitate electrolyte penetration.[45]

Powder X-ray diffraction (pXRD) was carried out to determine the crystallinity of the cathodes. All cathodes display similar diffraction patterns characteristic of the NTCDI active material, further confirming that the various binders do not affect the overall morphology of the redox-active component (Fig. 3f).[18] Furthermore, X-ray photoelectron spectroscopy (XPS) was utilized to probe the chemical composition of the surface regions of the cathodes. The survey spectra for all cathodes confirms the composition of O, N, and C elements (Fig. S20†). In particular, the XPS C 1s spectra of all pristine cathodes exhibited similar peaks at 288.8, 285.4, and 284.3 eV, corresponding to C=O, C–C, C=C, respectively (Fig. 3g). Additionally, a peak at 290.8 eV, attributed to C–F, was detected in the PVDF-based cathode due to the fluorine content in the binder.

Peeling tests (90°) were conducted to quantify the adherence of the various binders (Fig. 3h and Fig. S19†). The PVDF and POxa**P** cathodes exhibited adhesion forces of approximately 0.1 N, whereas the electrodes containing the gallol groups (POxa**G** and POxa**PG**) showed 5–15 times higher adhesion forces, due to the strong binding abilities of the gallol groups. Therefore, the gallol-based binders are expected to deliver enhanced performance over prolonged cycling in aqueous media.

Cell performance

The performance of the binders was tested by assembling coin cells (CR2032) using the electrode compositions (NTCDI : Super P : binder) as cathodes, zinc foil as the reference/counter electrode, and 2M $ZnSO_4$ as the electrolyte within a voltage range of 0.35 to 1.2 V (Fig. 4a). The charge–discharge voltage profiles at 0.01 A g^{-1} are all similar in shape, featuring well-defined charge and discharge peaks (Fig. 4b). Among the binders investigated, the POxa**PG**-based cathode achieves the highest capacity of 348 mAh g^{-1}. The similar profiles of all charge–discharge profiles suggests that the binders do not alter the redox activity of the NTCDI active material. Instead, the enhanced capacity observed with the dual-functional POxa**PG** binder is attributed solely to its improved binding and conductive properties. The voltage profiles indicate that oxidation and reduction occur at 0.76 V and 0.55 V, which was also affirmed by their corresponding differential capacity curves (Fig. 4c).

The rate performance of all cathodes was tested between current densities of 0.01 to 20 A g^{-1} (Fig. 4d and Table S1†). The PVDF-based cathode demonstrates discharge capacities from 258 to 113 mAh g^{-1} at rates of 0.01 to 20 A g^{-1}, respectively, aligning well with literature values.[18] At low current densities, cathodes prepared with the POxa**G** or POxa**P** binder show comparable capacities to those with the PVDF binder. However, at current densities of 2 A g^{-1} or higher, the performance of the POxa**P**-based cathode declines significantly, approaching near-zero capacities at 10 and 20 A g^{-1}. The poor high-rate capacities observed with the POxa**P** binder is attributed to the lack of sufficient binding groups. At high current densities, rapid ion insertion and extraction induce significant volume changes in the electrode. Binding groups are essential for accommodating these changes and preserving the electrode's mechanical integrity.[46] Without adequate binding groups, the POxa**P**-based cathodes likely experience electrode cracking or disintegration, resulting in diminished capacities.

The POxa**PG** cathode delivers the highest capacities across all tested current densities, highlighting the significant improvement that the POxa**PG** binder has on the NTCDI active material. Remarkably, a discharge capacity of 183 mAh g^{-1} is achieved at a current of 20 A g^{-1}, representing one of the highest reported capacities for organic carbonyl-based AZIBs at this current density. The superior rate capability of the POxa**PG**-based electrode is attributed to the synergistic effect of the gallol groups that improve binding with the electrode components and PEG groups that improve interfacial ion transport.

To determine if the improved performance with the POxa**PG** binder is a result of having both functionalities in the same polymer structure, we prepared cathodes comprising mixtures of POxa**G** (5 wt%) and POxa**P** (5 wt%), that were physically mixed during electrode fabrication (Fig. S23†). This cathode performed similarly to those using either POxa**G** or POxa**P** alone, indicating that optimal performance requires the binding and conductive functionalities to be covalently bonded onto the same polymer backbone, as shown in Fig. 2a. The poor performance of the POxa**G**/POxa**P** mixture is likely due to macrophase separation in the physical mixture, where differences in physical affinities among the two polymers leads to poor mixing, resulting in larger segregated domains. Additionally, separating the binding and conductive groups onto different polymer backbones hinders the formation of continuous ion and electron transport pathways. In contrast, a single polymer with integrated binding and conductive groups ensures a homogeneous and synergistic distribution, enhancing mechanical integrity, transport efficiency, and overall cathode performance.[47]

The electrochemical performances of the NTCDI cathodes with the PVDF or POxa**PG** binders were compared with other

Open Access Article. Published on 15 July 2025. Downloaded on 12/12/2025 10:12:56 PM.
This article is licensed under a Creative Commons Attribution-NonCommercial 3.0 Unported Licence.

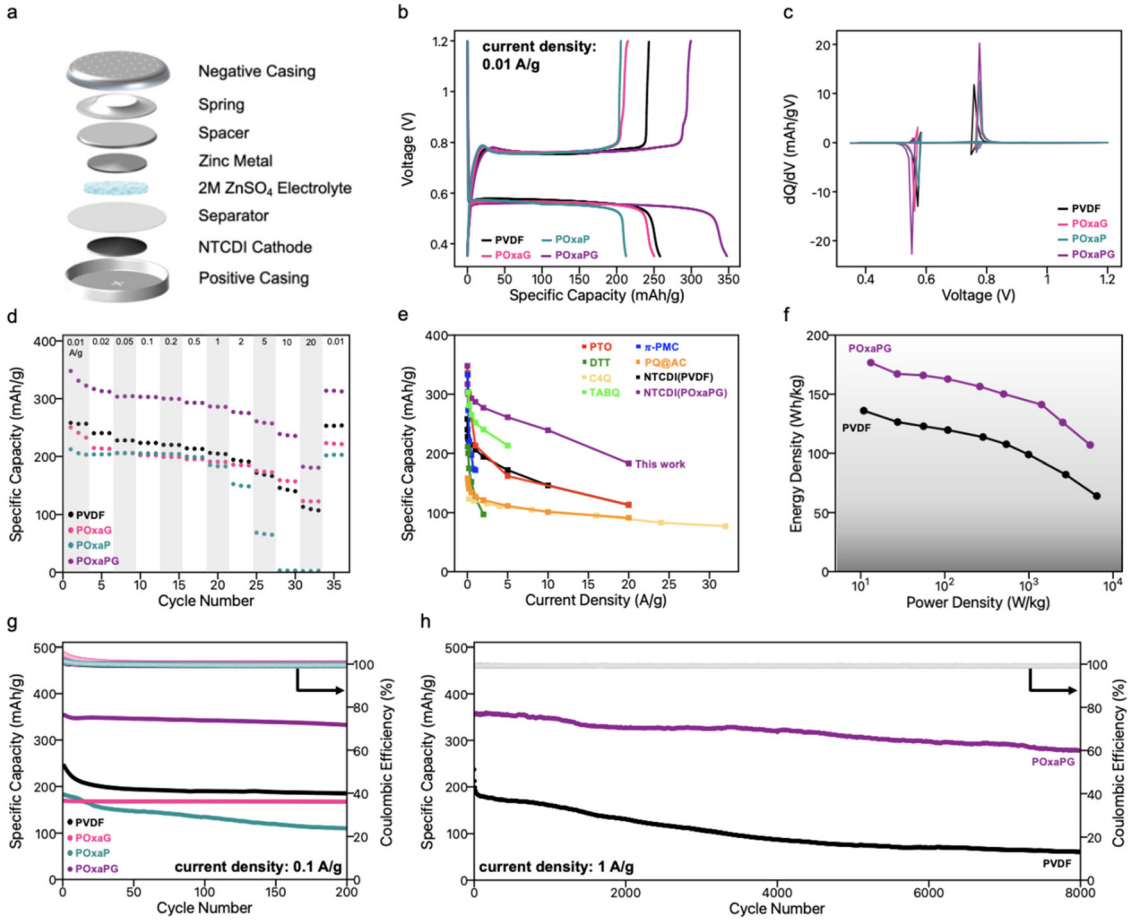

Fig. 4 Electrochemical performance of NTCDI cathodes in AZIBs with the binders tested in this study. (a) Schematic illustration of coin cell composition. (b) GCD profiles of cathodes at 0.01 A g^{-1}. (c) dQ/dV curves of cathodes. (d) Rate performance of cathodes. (e) Comparison of PVDF- and POxa**PG**-based cathodes with previously reported organic carbonyl materials. (f) Ragone plot of cathodes with PVDF or POxa**PG** binder. (g) Short-term cycling performance of NTCDI cathodes with the binders tested in this study at 0.1 A g^{-1}. (h) Long-term cycling performance of NTCDI cathodes with PVDF or POxa**PG** binder at 1 A g^{-1}.

previously reported organic carbonyl cathode materials in AZIBs, including PTO,[48] DTT,[49] C4Q,[50] TABQ,[51] π-PMC,[52] and PQ@AC[53] (Fig. 4e and Table S2†). The NTCDI cathode with the POxaPG binder delivers the highest capacity at 0.01 A g^{-1} and presents the best rate capability at high current densities up to 20 A g^{-1}.

Energy density and power density are two significant factors used to evaluate the electrochemical performance of energy storage devices. As such, the energy density and power density of cathodes using either PVDF or POxa**PG** as the binder were calculated using the rate performance data and the corresponding results were plotted as a Ragone plot (Fig. 4f). The POxa**PG** binder improves the energy density at all power densities compared to PVDF. At a power density of 13 W kg^{-1}, POxa**PG** achieves a specific energy density of 177 Wh kg^{-1}, which is comparable to the best recently reported AZIBs. Notably, even at an ultrahigh power density of 5.35 kW kg^{-1}, POxa**PG** maintains a high energy density of 107 Wh kg^{-1}, demonstrating a desired balance of energy and power density.

The cycling stabilities of the cathodes were tested at 0.1 A g^{-1} over 200 cycles (Fig. 4g and Table S1†). Cathodes with binders containing gallol moieties, POxa**G** and POxa**PG**, have the highest capacity retentions (99% and 94%, respectively), which is attributed to the strong binding abilities of the gallol groups. On the other hand, POxa**P** exhibited the lowest capacity retention (60%), as it lacks the binding groups necessary to preserve electrode integrity during extended cycling. The long-term cycling performance of POxa**PG** was assessed at 1 A g^{-1}, with PVDF included for accurate comparison (Fig. 4h). Impressively, the POxa**PG** binder maintains an excellent discharge capacity of ~358 mAh g^{-1} over 8000 cycles, achieving an impressive capacity retention of 78% and near-perfect coulombic efficiency, thus highlighting the exceptional stability of POxa**PG** during prolonged operation. In contrast, the cathode with PVDF exhibits a typical decline in capacity over cycling, resulting in a significantly lower capacity retention of only 26% after 8000 cycles. These findings clearly illustrate that the POxa**PG** binder not only enhances the system's delivered

 © 2025 The Author(s). Published by the Royal Society of Chemistry

Open Access Article. Published on 15 July 2025. Downloaded on 12/12/2025 10:12:56 PM.
This article is licensed under a Creative Commons Attribution-NonCommercial 3.0 Unported Licence.

capacity, but also significantly improves capacity retention during long-term cycling.

SEM measurements were conducted on the cathodes after 200 cycles at 0.1 A g^{-1} to verify the effects of the various binders on the structural integrity of the cathodes (Fig. 5a–d). The cycled cathodes containing either PVDF, POxa**G**, or POxa**PG** maintain relatively uniform surfaces with minimal aggregation or cracking. On the other hand, apparent cracks can be observed in the POxa**P**-based cathode, which is attributed to volume changes caused by the insertion and extraction of Zn^{2+} during charging/discharging. To further evaluate the physical stability, pristine cathodes were soaked in the aqueous electrolyte and monitored over several months (Fig. 5e and f). Within just 24 hours, the POxa**P** cathode completely delaminated from the current collector. In contrast, electrolyte solutions containing cathodes with PVDF, POxa**G**, or POxa**PG** as the binder remained clear and colourless, even after two months of soaking, indicating superior stability. Cracking in the cycled cathode and significant delamination during soaking emphasize the poor cycling stability and rate performance at high current densities of the POxa**P**-based cathode.

Charge storage mechanism

A detailed kinetic analysis was performed using cyclic voltammetry (CV) at scan rates ranging from 0.1 to 0.6 mV s^{-1} (Fig. 6a–d) to investigate the variations in rate capability and capacity retention associated with the various binders. The CV profiles show one pair of redox peaks, suggesting a one-step consecutive charge storage mechanism. All cathodes demonstrate increasing peak current densities and well-defined peak shapes with higher scan rates, indicating excellent electrochemical stability. Moreover, the CV profiles remain nearly identical regardless of the binder used, signifying that the binder choice has minimal impact on the redox activity of NTCDI. The charge storage contribution was analyzed using the equation $i = av^b$, where i represents the current response from the CV curve, v is the scan rate, and a and b are adjustable parameters. The slope, b, of the log (i) *vs.* log (v) curve indicates the dominant charge storage mechanism. A b value close to 1 indicates a surface capacitance behaviour, whereas a b value close to 0.5 indicates a diffusion-controlled process.[54] Both the anodic and cathodic peaks follow similar trends, with PVDF exhibiting the highest b value, while cathodes containing gallol moieties (POxa**G** and POxa**PG**) show the lowest b values (Fig. 6e and f). This signifies that the addition of the gallol moiety in the binder increases the diffusion contribution of the charge storage process.

In addition, the ratio of the capacitance contribution (k_1v) and the diffusion control contribution (k_2v) can be approximately calculated according to the equation $i = k_1v + k_2v^{1/2}$.[55] As the sweep rate increases from 0.1 to 0.6 mV s^{-1}, the capacitive-controlled contribution gradually increases for all binders (Fig. 6g–j). These results indicate that the storage mechanism is more capacitive-based for the PVDF-based cathode, which is known to lead to high rate capability and fast kinetics. Interestingly, the cathodes with the POxa**G**, POxa**P**, and POxa**PG** electrodes are more diffusion-controlled, whose charge storage mechanism mainly involves the insertion of Zn-ions. The relatively low capacitive contribution of the POxa**G**, POxa**P**, and POxa**PG** electrodes indicates that solid-state diffusion is the rate limiting step. Therefore, the increase in the specific capacities of the POxa**PG**-based cathode is not due to enhanced surface-controlled capacitive effects resulting

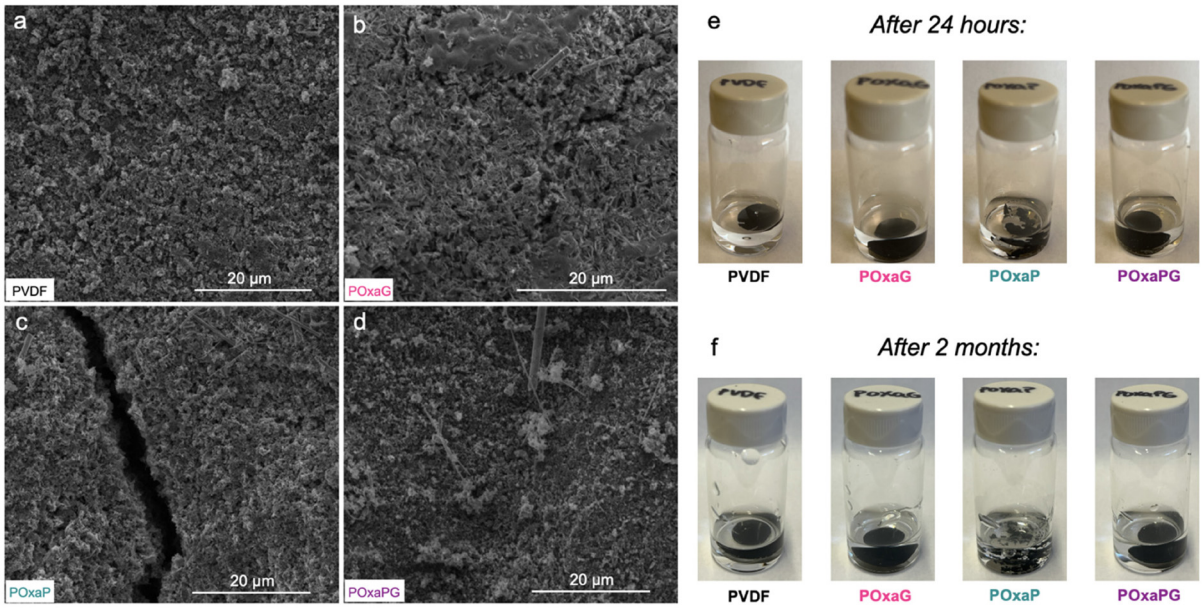

Fig. 5 SEM images of (a) PVDF-, (b) POxa**G**-, (c) POxa**P**-, or (d) POxa**PG**-based cathodes after 200 cycles at 0.1 A g^{-1}. Images of pristine, uncycled cathodes after soaking in 2M $ZnSO_4$ aqueous electrolyte for (e) 24 hours and (f) 2 months.

Open Access Article. Published on 15 July 2025. Downloaded on 12/12/2025 10:12:56 PM.
This article is licensed under a Creative Commons Attribution-NonCommercial 3.0 Unported Licence.

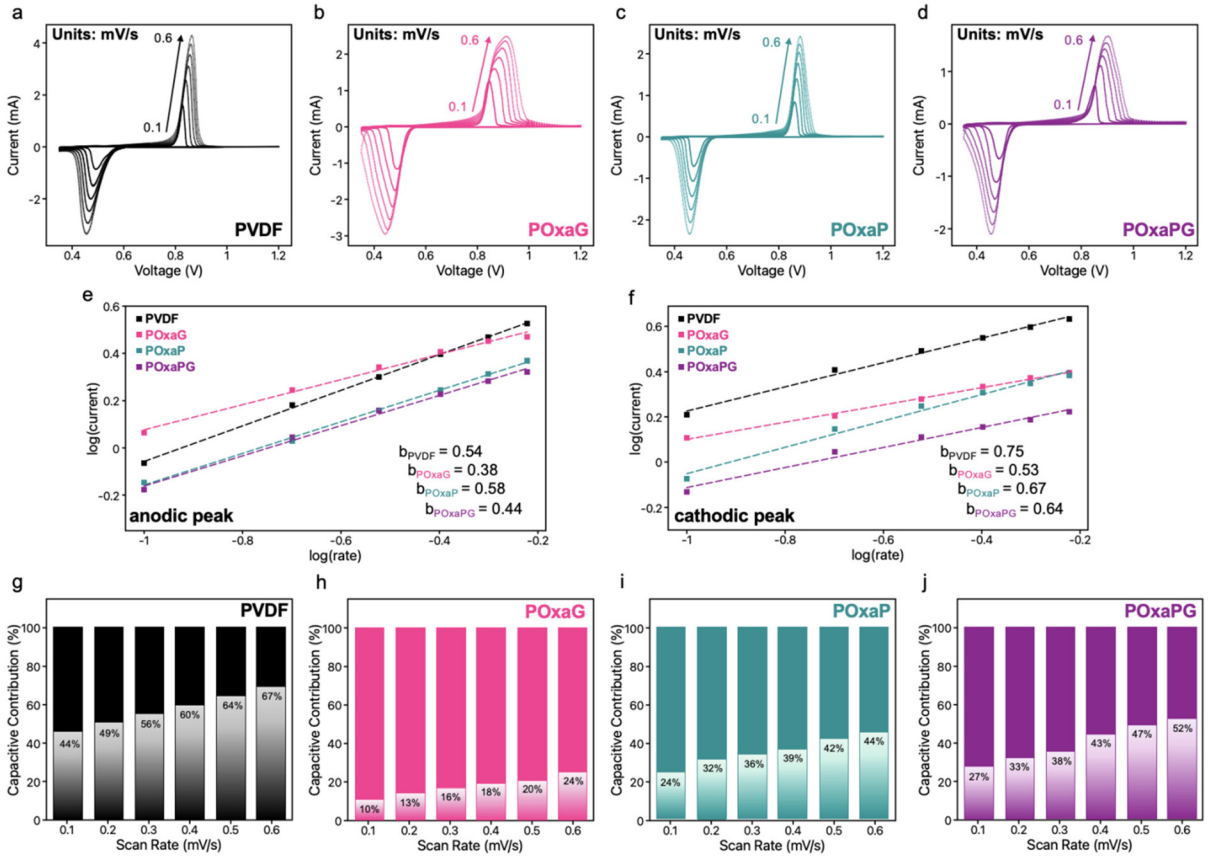

Fig. 6 CV curves of NTCDI cathodes with (a) PVDF, (b) POxa**G**, (c) POxa**P**, or (d) POxa**PG** binder at different scan rates. Corresponding plots of log (rate) *versus* log (current) peak for (e) anodic and (f) cathodic peak. The capacitive contribution at different scan rates of NTCDI cathodes with (g) PVDF, (h) POxa**G**, (i) POxa**P**, or (j) POxa**PG** binder.

from a larger specific surface area. Instead, we hypothesize that it results from strong binding interactions between the gallol groups and electrode particles, which creates fast pathways for electron transport, as well as the PEG groups, which improve ion diffusion kinetics. By incorporating both gallol and PEG groups, the POxa**PG**-based cathode achieves the highest rate performance by facilitating electron transport and ion diffusion efficiency.

Interface evolution

Electrochemical impedance spectroscopy (EIS) was used to determine the reaction kinetics of Zn^{2+} in the batteries after cycling and investigate more detailed reasons for the high rate performance of the POxa**PG**-based cathode. The Nyquist plots consist of a semi-circle in the high-frequency region (charge transfer resistance) and a linear tail extending into the low-frequency region (ion diffusion) (Fig. 7a). The POxa**PG**-based cathode exhibits the lowest internal resistance and charge transfer resistance among the four cathodes. The Zn-ion diffusion coefficient ($D_{Zn^{2+}}$) can be calculated from the low-frequency region of the Nyquist plots (eqn (S4) and (S5)†), where the $D_{Zn^{2+}}$ is evaluated using the relationship between the real part of the impedance and low-frequency (Fig. 7b).[56] The POxa**PG**-based cathode exhibits the highest $D_{Zn^{2+}}$ value (7.54×10^{-9} cm^2 s^{-1}) among the four binders studied. The smaller slope of the POxa**PG**-based cathode in the linear region corresponds to faster ion diffusion (Table S1†). In contrast, the PVDF-based cathode has the lowest $D_{Zn^{2+}}$ value (1.01×10^{-10} cm^2 s^{-1}), highlighting the significant ability of the POxa**PG** binder to enhance Zn-ion diffusion kinetics. The rapid Zn^{2+} diffusivity observed with the POxa**PG** binder allows this system to achieve excellent rate properties, aligning well with the rate capability data obtained from the electrochemical tests.

The pXRD patterns of the cathodes in the discharged state all exhibit a new prominent diffraction peak at approximately $2\theta = 8.8°$, indicative of Zn^{2+} insertion into NTCDI (Fig. 7c).[43,57] No other changes (appearance or disappearance of peaks) are observed, suggesting that the discharge process is unaffected by the choice of binder.

XPS was also conducted on the C and Zn elements to analyze the chemical composition of the surface and near-surface regions of the cathodes in various states. The C 1s spectra shows four signals at 288.8, 286.4, 285.5, 285.3 eV in the pristine state, which belong to the C═O, C–O, C–C, and C═C groups, respectively (Fig. 7d, e and Fig. S21†). Due to the

 © 2025 The Author(s). Published by the Royal Society of Chemistry

Open Access Article. Published on 15 July 2025. Downloaded on 12/12/2025 10:12:56 PM.
This article is licensed under a Creative Commons Attribution-NonCommercial 3.0 Unported Licence.

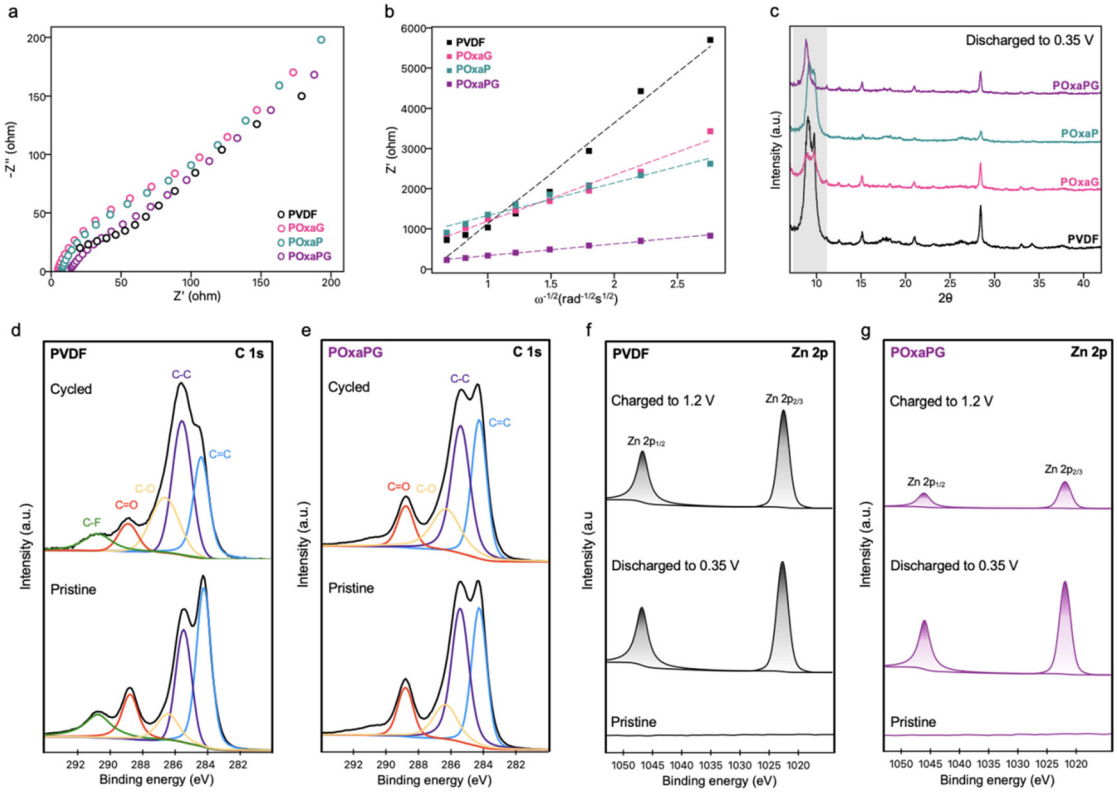

Fig. 7 (a) Nyquist plots of NTCDI cathodes with the binders tested in this study after the 25th cycle. (b) Linear diagrams of Z' *versus* $\omega^{-1/2}$ of the NTCDI cathodes with the binders tested in this study at the low-frequency region. (c) The pXRD patterns of cathodes using PVDF, POxa**G**, POxa**P**, or POxa**PG** binder in the discharged state. The C 1s spectra of NTCDI cathode with (d) PVDF or (e) POxa**PG** binder in the pristine or cycled state. The Zn 2p spectra of NTCDI cathodes with (f) PVDF or (g) POxa**PG** binder in the pristine, discharged, or charged state in the first cycle.

addition of fluorine in the PVDF binder, the PVDF-based cathode also contains a signal for C–F at 290.5 eV. Upon cycling, all peaks remain with minimal changes in their peak areas. This structural evolution highlights the highly reversible redox reaction of NTCDI and indicates that the choice of binder does not impact NTCDI's ability to participate in the redox reactions required for Zn-ion storage. The Zn 2p spectra exhibit two strong peaks with binding energies of 1022.6 and 1045.6 eV in the discharged state (0.35 V), corresponding to the Zn $2p_{3/2}$ and Zn $2p_{1/2}$ peaks, respectively (Fig. 7f, g and Fig. S22†). Upon recharging to 1.2 V, these peaks significantly diminish for the POxa**PG**-based electrode, indicating extremely efficient Zn^{2+} ion removal from NTCDI. In contrast, the peaks for the PVDF-based cathode remain largely unchanged, reflecting poor Zn^{2+} ion removal. These findings align with the earlier results discussed in this paper, reinforcing that the POxa**PG** binder improves Zn^{2+} transport within the cathode.

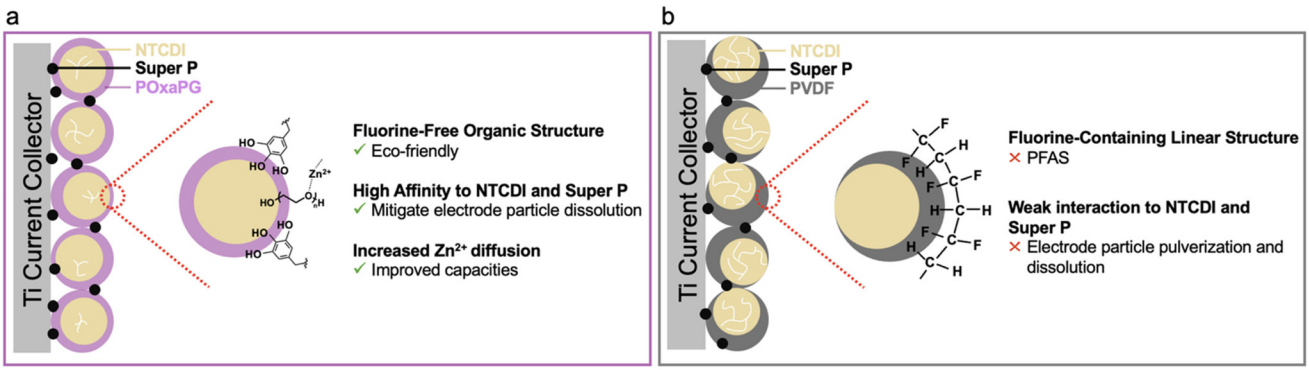

Fig. 8 Schematic illustration of cathode properties with either (a) POxa**PG** or (b) PVDF as the binder.

Open Access Article. Published on 15 July 2025. Downloaded on 12/12/2025 10:12:56 PM.
This article is licensed under a Creative Commons Attribution-NonCommercial 3.0 Unported Licence.

Based on the experimental results obtained thus far, we propose a three-fold mechanism to explain how the POxa**PG** binder improves both the environmental sustainability and electrochemical stability of carbonyl-based cathodes for AZIBs. First, POxa**PG** is fluorine-free and does not contribute to the accumulation of PFAS in the environment. Second, the high gallol content in POxa**PG** induces strong interactions between POxa**PG** and NTCDI particles, which mitigates their dissolution into the electrolyte during cycling. Finally, the presence of PEG groups in POxa**PG** enhances Zn^{2+} diffusion, leading to increased capacities (Fig. 8a). To put this into context with the canonical PVDF binder, PVDF is a fluorine-bearing linear structure, and our data has shown that PVDF forms weak interactions between the binder and electrode particles, leading to NTCDI particle pulverization and significant deterioration in the electrochemical performance of organic AZIBs.

Conclusions

We have developed a novel multifunctional binder (POxa**PG**) that significantly enhances the performance of organic AZIBs. Including gallol groups improves adhesion to the NTCDI active material through hydrogen bonding and π–π interactions, while the PEG groups enhance ionic conductivity. POxa**PG**-based cathodes have higher capacities, better cycling stability, and superior rate performance compared to the commercial PVDF binder, as well as control experiments using the POxa**G** and POxa**P** homopolymers. This is attributed to POxa**PG**'s improved adhesion, conductivity, and stability. The combination of the NTCDI active material and the POxa**PG** binder achieves one of the highest reported capacities in aqueous zinc-ion batteries at a high current density (20 A g^{-1}). Comprehensive investigations utilizing X-ray photoelectron spectroscopy (XPS), electrochemical impedance spectroscopy (EIS), and cyclic voltammetry (CV) demonstrate that the improved performance of AZIBs using the POxa**PG** binder is a result of improved Zn^{2+} diffusion efficiency. This well-designed, straightforward, and practical approach offers many new opportunities for conceiving new conductive, environmentally-friendly binders with reliable adhesion in aqueous electrolytes for organic AZIBs and batteries beyond Li.

Author contributions

D. S. S. supervised the project. A. M. B. conceived the idea and conducted the experiments. J.T.L., V. L., and K. L. P. assisted with material characterization and data analysis. A. M.B. wrote the manuscript, with comments and revisions from all the authors.

Conflicts of interest

There are no conflicts to declare.

Data availability

The data supporting this article has been included as part of the article or included in the ESI.†

Acknowledgements

This work was supported by the National Sciences and Engineering Research Council of Canada (NSERC), the Canadian Foundation for Innovation, and the Ontario Research Fund. AMB is grateful for an Ontario Graduate Scholarship, JTL for an NSERC PGS-D, and VL for an NSERC PGS-D. The authors acknowledge the support of the Government of Canada's New Frontiers in Research Fund (NRF), CANSTOREnergy project NFRFT-2022-00197. The authors thank Prof. H. Tran for use of the mechanical tester, and A. Watson for assistance with the peel tests.

References

1 J.-M. Tarascon and M. Armand, *Nature*, 2001, **414**, 359.
2 Y. Chen, Y. Kang, Y. Zhao, L. Wang, J. Liu, Y. Li, Z. Liang, X. He, X. Li, N. Tavajohi and B. Li, *J. Energy Chem.*, 2021, **59**, 83.
3 M. Li, J. Lu, Z. Chen and K. Amine, *Adv. Mater.*, 2018, **30**, 1800561.
4 G. Fang, J. Zhou, A. Pan and S. Liang, *ACS Energy Lett.*, 2018, **3**, 2480.
5 E. Grignon, A. M. Battaglia, T. B. Schon and D. S. Seferos, *iScience*, 2022, 104204.
6 X. Zeng, J. Mao, J. Hao, J. Liu, S. Liu, Z. Wang, Y. Wang, S. Zhang, T. Zheng, J. Liu, P. Rao and Z. Guo, *Adv. Mater.*, 2021, **33**, 2007416.
7 S. Liu, J. Mao, W. K. Pang, J. Vongsvivut, X. Zeng, L. Thomsen, Y. Wang, J. Liu, D. Li and Z. Guo, *Adv. Funct. Mater.*, 2021, **31**, 2104281.
8 X. Zeng, J. Liu, J. Mao, J. Hao, Z. Wang, S. Zhou, C. D. Ling and Z. Guo, *Adv. Energy Mater.*, 2020, **10**, 1904163.
9 Q. Yang, Q. Li, Z. Liu, D. Wang, Y. Guo, X. Li, Y. Tang, H. Li, B. Dong and C. Chi, *Adv. Mater.*, 2020, **32**, 2001854.
10 C. Han, H. Li, R. Shi, T. Zhang, J. Tong, J. Li and B. Li, *J. Mater. Chem. A*, 2019, **7**, 23378.
11 S. Y. An, T. B. Schon, B. T. McAllister and D. S. Seferos, *EcoMat*, 2020, **2**, e12055.
12 L. Zhu, G. Ding, L. Xie, X. Cao, J. Liu, X. Lei and J. Ma, *Chem. Mater.*, 2019, **31**, 8582.
13 R. Shi, S. Jiao, Q. Yue, G. Gu, K. Zhang and Y. Zhao, *Exploration*, 2022, **2**, 20220066.
14 J. Lee, H. Kim and M. J. Park, *Chem. Mater.*, 2016, **28**, 2408.
15 H. Kim, J. E. Kwon, B. Lee, J. Hong, M. Lee, S. Y. Park and K. Kang, *Chem. Mater.*, 2015, **27**, 7258.
16 Y. T. Yokoji, H. Matsubara and M. Satoh, *J. Mater. Chem. A*, 2014, **2**, 19347.

 © 2025 The Author(s). Published by the Royal Society of Chemistry

Open Access Article. Published on 15 July 2025. Downloaded on 12/12/2025 10:12:56 PM.
This article is licensed under a Creative Commons Attribution-NonCommercial 3.0 Unported Licence.

17 L. Sieuw, A. Jouhara, É. Quarez, C. Auger, J.-F. Gohy, P. Poizot and A. Vlad, *Chem. Sci.*, 2019, **10**, 418.
18 X. Wang, L. Chen, F. Lu, J. Liu, X. Chen and G. Shao, *ChemElectroChem*, 2019, **6**, 3644.
19 B. Pan, J. Huang, Z. Feng, L. Zeng, M. He, L. Zhang, J. T. Vaughey, M. J. Bedzyk, P. Fenter, Z. Zhang, A. K. Burrell and C. Liao, *Adv. Energy Mater.*, 2016, **6**, 1600140.
20 Z. Song, Y. Qian, T. Zhang, M. Otani and H. Zhou, *Adv. Sci.*, 2015, **2**, 1500124.
21 Z. Song, Y. Qian, X. Liu, T. Zhang, Y. Zhu, H. Yu, M. Otani and H. Zhou, *Energy Environ. Sci.*, 2014, **7**, 4077.
22 Z. Zhu, M. Hong, D. Guo, J. Shi, Z. Tao and J. Chen, *J. Am. Chem. Soc.*, 2014, **136**, 16461.
23 W. Wei, L. Li, L. Zhang, J. Hong and G. He, *Electrochem. Commun.*, 2018, **90**, 21.
24 Y. Han, Y. Liu, Y. Zhang, X. He, X. Fu, R. Shi, S. Jiao and Y. Zhao, *Adv. Mater.*, 2025, **37**, 2412447.
25 L. M. Lv, R. Zhao, Z. Hu, J. Yang, X. Han, Y. Wang, C. Wu and Y. Bai, *Energy Environ. Sci.*, 2024, **17**, 4871.
26 H. Chen, M. Ling, L. Hencz, H. Y. Ling, G. Li, Z. Lin, G. Liu and S. Zhang, *Chem. Rev.*, 2018, **118**, 8936.
27 M. Wang, K. Liu, J. Yu, Q. Zhang, Y. Zhang, M. Valix and D. C. W. Tsang, *Glob. Chall.*, 2023, **7**, 2200237.
28 H. Y. Ling, C. Wang, Z. Su, S. Chen, H. Chen, S. Qian, D.-S. Li, C. Yan, M. Kiefel, C. Lai and S. Zhang, *Energy Environ. Mater.*, 2021, **4**, 263.
29 Y. Ding, X. Zhong, C. Yuan, L. Duan, L. Zhang, Z. Wang, C. Wang and F. Shi, *ACS Appl. Mater. Interfaces*, 2021, **13**, 20681.
30 J. N. Jaikrajang, W. Kao-Ian, T. Muramatsu, R. Chanajaree, T. Yonezawa, Z. Y. Al Balushi, S. Kheawhom and R. Cheacharoen, *ACS Appl. Energy Mater.*, 2021, **4**, 7138.
31 M.-H. Ryou, J. Kim, I. Lee, S. Kim, Y. K. Jeong, S. Hong, J. H. Ryu, T.-S. Kim, J.-K. Park, H. Lee and J. W. Choi, *Adv. Mater.*, 2013, **25**, 1571.
32 H. Zhao, Y. Wei, C. Wang, R. Qiao, W. Yang, P. B. Messersmith and G. Liu, *ACS Appl. Mater. Interfaces*, 2018, **10**, 5440.
33 S. Ko, M.-J. Baek, T.-U. Wi, J. Kim, C. Park, D. Lim, S. J. Yeom, K. Bayramova, H. Y. Lim, S. K. Kwak, S. W. Lee, S. Jin, D. W. Lee and H.-W. Lee, *ACS Mater. Lett.*, 2022, **4**, 831.
34 A. M. Battaglia, E. Grignon, J. T. Liu and D. S. Seferos, *Small*, 2024, **20**, 2405118.
35 C. Jin, J. Nai, O. Sheng, H. Yuan, W. Zhang, X. Tao and X. W. Lou, *Energy Environ. Sci.*, 2021, **14**, 1326.
36 K. Zhan, C. Kim, K. Sung, H. Ejima and N. Yoshie, *Biomacromolecules*, 2017, **18**, 2959.
37 K. K. Rajeev, W. Jang, S. Kim and T.-H. Kim, *ACS Appl. Energy Mater.*, 2022, **5**, 3166.
38 H. A. Lee, M. Shin, J. Kim, J. W. Choi and H. Lee, *Adv. Mater.*, 2021, **33**, 2007460.
39 X. Lin, L. Yu, Y. Wen, L. Qi, S. Wang, H. Liu, X. Xu and C. Chen, *Cell Rep. Phys. Sci.*, 2023, **4**, 101730.
40 F. Liu, Y. Long, Q. Zhao, X. Liu, G. Qiu, L. Zhang, Q. Ling and H. Gu, *Polymer*, 2018, **143**, 212.
41 J. A. Love, J. P. Morgan, T. M. Trnka and R. H. Grubbs, *Angew. Chem., Int. Ed.*, 2002, **41**, 4035.
42 D. Yao, J. Feng, J. Wang, Y. Deng and C. Wang, *J. Power Sources*, 2020, **463**, 228188.
43 K. R. Kasinathan, M. Marinaro, P. Axmann and M. Wohlfahrt-Mehrens, *Energy Technol.*, 2018, **6**, 2256.
44 M. Seydou, J. Teyssandier, N. Battaglini, G. T. Kenfack, P. Lang, F. Tielens, F. Maurel and B. Diawara, *RSC Adv.*, 2014, **4**, 25698.
45 Y. Shi, X. Zhou and G. Yu, *Acc. Chem. Res.*, 2017, **50**, 2642.
46 M. Zhou, X. Zhou, Y. Yang, H. Yin, Y. Lei, S. Liang and G. Fang, *Chem. Eng. J.*, 2024, **497**, 154916.
47 H. An, X. Li, C. Chalker, M. Stracke, R. Verduzco and J. L. Lutkenhaus, *ACS Appl. Mater. Interfaces*, 2016, **8**, 28585.
48 Z. Guo, Y. Ma, X. Dong, J. Huang, Y. Wang and Y. Xia, *Angew. Chem., Int. Ed.*, 2018, **57**, 11737.
49 Y. Wang, C. Wang, Z. Ni, Y. Gu, B. Wang, Z. Guo, Z. Wang, D. Bin, J. Ma and Y. Wang, *Adv. Mater.*, 2020, **32**, 2000338.
50 Q. Zhao, W. Huang, Z. Luo, L. Liu, Y. Lu, Y. Li, L. Li, J. Hu, H. Ma and J. Chen, *Sci. Adv.*, 2018, **4**, eaao1761.
51 Z. Lin, H.-Y. Shi, L. Lin, X. Yang, W. Wu and X. Sun, *Nat. Commun.*, 2021, **12**, 4424.
52 H. Zhang, Y. Fang, F. Yang, X. Liu and X. Lu, *Energy Environ. Sci.*, 2020, **13**, 2515.
53 B. Yang, Y. Ma, D. Bin, H. Lu and Y. Xia, *ACS Appl. Mater. Interfaces*, 2021, **13**, 58818.
54 P. Simon, Y. Gogotsi and B. Dunn, *Science*, 2014, **343**, 1210.
55 V. Augustyn, P. Simon and B. Dunn, *Energy Environ. Sci.*, 2014, **7**, 1597.
56 P. Hu, T. Zhu, X. Wang, X. Wei, M. Yan, J. Li, W. Luo, W. Yang, W. Zhang, L. Zhou, Z. Zhou and L. Mai, *Nano Lett.*, 2018, **18**, 1758.
57 A. Moezzi, M. B. Cortie and A. M. McDonagh, *Dalton Trans.*, 2013, **42**, 14432.

© 2025 The Author(s). Published by the Royal Society of Chemistry